GI-XRD measurements of thin film samples using a 2D detector and 2D-SAXS/WAXS attachment

Shintaro Kobayashi* and Katsuhiko Inaba**

1. Introduction

In our previous report[1], we introduced the concept of GI-XRD (grazing-incidence X-ray diffraction) with a 2-dimensional (2D) detector for thin film samples[2, 3]. However, it seems we have not fully explained how well a 2D-SAXS/WAXS (reflection) attachment works in GI-XRD with a 2D detector.

So, we decided to briefly review the usefulness of this attachment together with up-to-date applications of functional thin films by GI-XRD using a HyPix-3000 2D detector with this attachment.

2. 2D-SAXS/WAXS (reflection) attachment

2.1. A general view of the attachment

First, let us examine the components of the 2D-SAXS/WAXS (reflection) attachment. GI-XRD geometry with a 2D detector is shown in Fig. 1[1]. Figure 2 shows a photo of the 2D-SAXS/WAXS (reflection) attachment installed on a SmartLab system with a HyPix-3000 2D detector, and Fig. 3 shows the details of this attachment. A sample is placed on the center of a sample stage. This attachment is composed of two major functional parts; 1) Beam stop and 2) Scattering shield.

A position-adjustable reflection beam stop of variable sizes is installed to suppress the influence of undesirable X-ray signals from the direct beam and the sample surface (total external reflection). Since this component is clamped by magnets with pin-guides, it can be easily detached and remounted with high positional reproducibility.

A scattering shield suppresses the contribution of air-scattering caused by the incident X-rays or of scattering caused by the sample surface, and its position can be shifted with a guide consisting of two rails. A micro screw enables fine tuning of the distance of the scattering shield above the sample surface. It can be retracted and clamped by magnets to the highest position far from the samples making sample recovery easy and safe. The air-scattering shield can be used in two modes: as a knife edge anti-scattering shield or as a pinhole slit with an air-scattering shield. The knife edge anti-scattering shield is adopted for X-ray Reflectivity (XRR) measurements with line-focus incident optics. The simultaneous use of an air-scattering shield and a pinhole slit with an anti-scattering shield is employed for GI-XRD with a 2D detector[1]; this configuration is called as “aperture slit” (patent pending).

In the next section, how this aperture slit will work well for GI-XRD with a 2D detector will be explained.

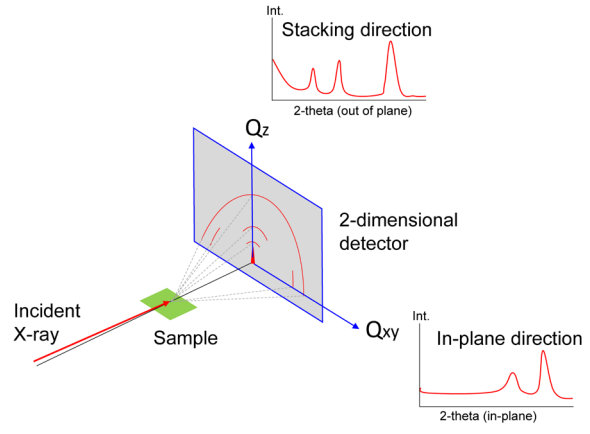

Fig. 1. Geometry of GI-XRD with a 2-dimentional detector.

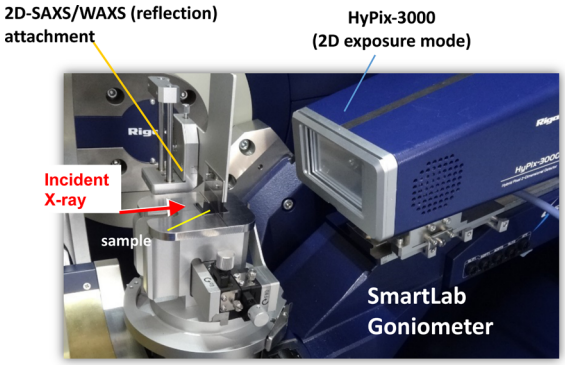

Fig. 2. 2D-SAXS/WAXS (reflection) attachment installed on a “SmartLab with a HyPix-3000” system.

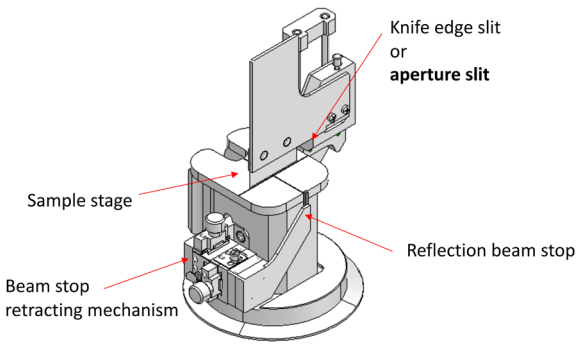

Fig. 3. Details of the 2D-SAXS/WAXS (reflection) attachment.

* Application Laboratories, Rigaku Corporation.
** X-ray Research Laboratory, Rigaku Corporation.

2.2. Aperture slit for GI-XRD with 2D detector

In general GI-WAXS measurements with a 2D detector, the incident X-rays should be converted to point shape using a collimator or focusing optics[1, 4–7]. Using a point-shaped incident beam limits the spatial broadening of the diffraction spots observed by the 2D detector, and thus enhances spatial resolution. For grazing incidence geometry, however, the exposed area on the sample surface is wide[1, 7–9], thus, diffracted signals will broaden at higher 2θ angles (to 90° for θd) as is schematically shown in Fig. 4. This is inevitable even if a pinhole collimator is employed for the incident optics as can be seen clearly in Fig. 5(a) and (b).

Figure 5(a) is the same figure shown as Fig. 7. in Ref. 1, employing this aperture slit, for GI-WAXS measurement with a 2D detector (exposure time of 30 min) of a pentacene thin film on a Si substrate[1, 10]. Figure 5(b) is from the same sample but using a pinhole collimator of ϕ0.3 mm in the incident optics without using an aperture slit with an exposure time of 60 min. By employing "aperture slit", the diffraction signals are clearly observed as spots with a high signal-to-noise ratio.

The aperture slit is a combination of an air-scattering shield and a pinhole slit. The pinhole slit is designed to be positioned at the center of the goniometer, so that diffracted signals passing through this pinhole, which acts as a pseudo-focal point, are detected by the 2D detector. By employing this pinhole slit, the sample size effect shown in Fig. 4 can be greatly suppressed. Moreover, a line-shaped incident beam can be employed for GI-XRD measurements when this aperture slit and an incident parallel slit collimator (PSC) are installed. The employment of a line-shaped incident beam, instead of a point-shaped beam, increases the irradiated area on the sample surface along the direction perpendicular to the incident beam path. However, since a PSC is installed at the incident optic side, it creates the same situation as if the sample were irradiated with multiple pinhole collimators. Also, a pinhole slit at the goniometer center limits the diffraction signals without causing broadening at the 2D detector face. Therefore, the combined use of a PSC and aperture slit can collect the diffraction signals from a wide irradiated range

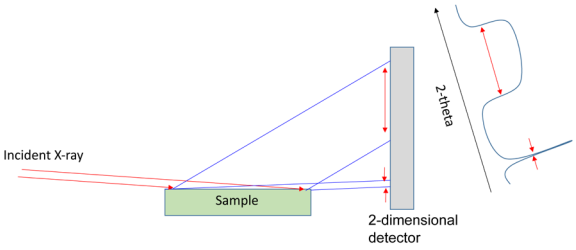

Fig. 4. The sample size effect of GI-XRD geometry with a 2-dimentional detector.

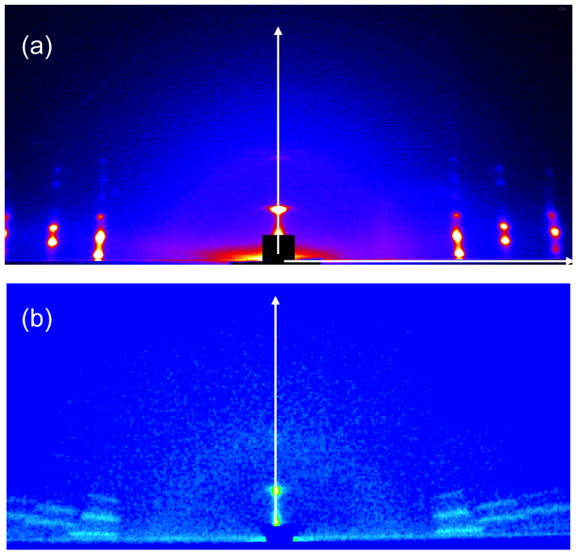

Fig. 5. GI-WAXS images of a pentacene thin film on a Si substrate.
(a) Measured with incident line-beam and "aperture slit".
(b) Measured with ϕ0.3 mm pinhole at incident optic.

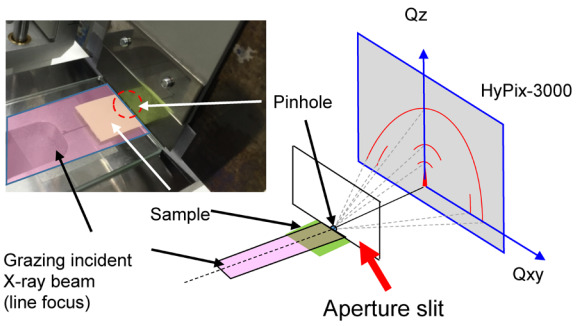

Fig. 6. Geometry for GI-WAXS measurement with 2D detector using "aperture slit".

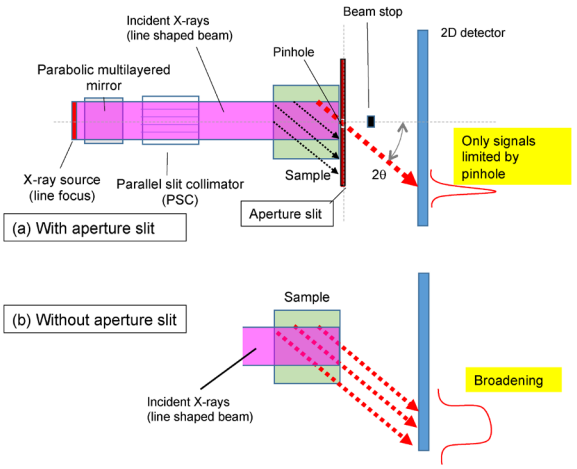

Fig. 7. A schematic illustration of 2D GI-WAXS measurement with line-shaped incident beams, viewed from a sample surface side.
(a) Using aperture slit together with incident parallel slit collimator.
(b) Without using aperture slit.
(Red dotted lines are denoted to the diffracted signals from sample.)

of a sample surface without causing broadening at the 2D detector face and without any aberration in 2θ positions. This situation is schematically explained in Fig. 7, comparing GI-WAXS geometry using aperture slit together with incident PSC (Fig. 7(a)), and without using aperture slit (Fig. 7(b)).

Collecting diffraction signals from a wide range of a sample surface is more significant for Grazing-Incident In-Plane XRD (GI-IP-XRD) signals, since these signals are less likely to be stopped by an anti-scattering shield.

3. Application to functional materials

A recent application example of a 2D GI-WAXS image using the 2D-SAXS/WAXS (reflection) attachment on a SmartLab system equipped with a HyPix-3000 2D detector is shown in this section, which explores the molecular orientation of organic semiconductor thin films.

Organic semiconductor thin films have been attracting a great deal of attention as next-generation, light-weight and flexible solar cells because they can be produced by low-cost ink-jet printing techniques. Energy conversion efficiency of more than 10% has been reported with organic solar cells. Control of the molecular arrangement of organic semiconductor thin films is considered to be indispensable for further improvement of their efficiency[11].

PNTz4T as a *p*-type organic semiconductor polymer thin film[12), (13], discovered by a research group at Riken, Japan. Its molecular structure is shown in Fig. 8.

Figure 9 shows a 2D WAXS image for the composite thin films of PNTz4T and PC71BM, as an *n*-type organic semiconductor, grown on a ZnO/ITO substrate[14]. (exposure time: 30 min) XRD profiles extracted from this image along the film stacking and the in-plane directions are shown in Fig. 10(a) and (b).

A clear spot and peak which originated from the "face-on" molecular configurations of $\pi-\pi$ stacking of the PNTz4T molecular sheets[14] (schematically shown in Fig. 11) can be observed in these figures. The distance of $\pi-\pi$ stacking of PNTz4T molecular sheets was calculated as 3.63 Å from the peak position in Fig. 10(a). This distance is shorter than those reported for common organic semiconductor thin films[15), (16]. The direction of molecular arrangements and the distance between these molecular sheets are expected to be greatly correlated with the conductivity of electrical holes. The fact that molecular sheets are arranged to stack parallel to the sample surface suggests it would be favorable to fabricate *p*–*n* junctions parallel to the device surface plane. The shorter stacking distance of the molecular sheets is expected to be favorable for the higher mobility of electrical holes. These two findings are evidence for the promising properties of this material for organic solar cells of higher efficiency in future.

Also, a clear spot and peak which originated from a lamellar structure of PNTz4T can be observed in the GI-SAXS region, close to the origin of reciprocal space

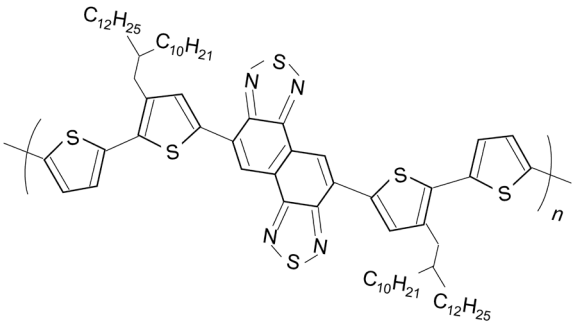

Fig. 8. Molecular structure of PNTz4T.

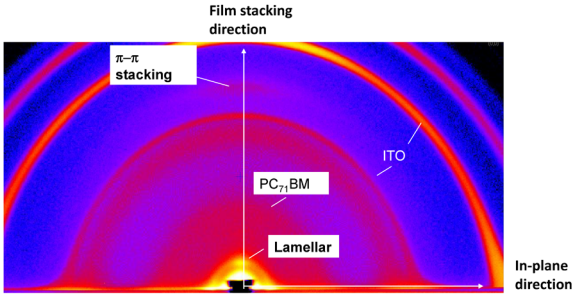

Fig. 9. A 2D GI-WAXS image of a PNTz4T/PC71BM composite film on a ZnO/ITO substrate.

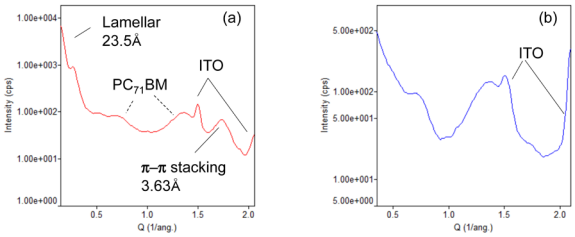

Fig. 10. XRD profiles extracted from the image in Fig. 9. (a) Along the stacking direction. (b) Along the in-plane direction.

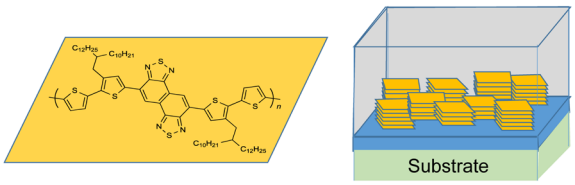

Fig. 11. A molecular model of PNTz4T molecular sheet (left) and preferred orientation of $\pi-\pi$ stacking (face-on arrangement) of the molecular sheets (right).

coordinates in Fig. 9 and Fig. 10(a). The distance of lamellar stacking was calculated as 23.2 Å from the peak position in Fig. 10(a).

4. Conclusion

Details of the GI-SAXS/WAXS (reflection) attachment on a SmartLab system equipped with a HyPix-3000 2D detector were explained. This attachment on a SmartLab system equipped with a

HyPix-3000 2D detector is a powerful tool for the analysis of functional thin film samples.

The authors greatly appreciate Professor Dr. Itaru Osaka from Hiroshima University for providing us advanced samples and details about them. We were also able to learn about the advanced technology of organic-solar cell material through this measurement.

References

(1) S. Kobayashi and K. Inaba: *Rigaku Journal (English version)*, **32** (2016), No. 2, 1−5.
(2) K. Inaba: *Rigaku Journal (English version)*, **33** (2017), No.1, 10−14.
(3) K. Inaba, S. Kobayashi, K. Uehara, A. Okada, S. L. Reddy and T. Endo: *Adv. Mater. Phys. Chem*., **3** (2013), 72−89. (Open Access) http://dx.doi.org/10.4236/ampc.2013.31A010
(4) Y. Shiramata: *Rigaku Journal (English version)*, **32** (2016), No. 1, 3−9.
(5) K. Nagao and E. Kagami: *Rigaku Journal (English version)*, **27** (2011), No. 2, 6−14.
(6) O. Engler and V. Randle: "*Introduction to Texture Analysis —Macrotexture, Microtexture, and Orientation Mapping—*", CRC Press (2010).
(7) M. Birkholz: "*Thin Film Analysis by X-Ray Scattering*", Wiley-VCH Verlag GmbH & Co., (2006).
(8) S. Kobayashi and K. Inaba: *Rigaku Journal (English version)*, **32** (2016), No. 2, 1−5.
(9) T. Mitsunaga: *Rigaku Journal (English version)*, **25** (2009), No. 1, 7−12.
(10) H. Yoshida, K. Inaba and N. Sato: *Appl. Phys. Lett*., **90** (2007), 181930-1−181930-3.
(11) T. Okamoto: *Rigaku Journal (English version)*, **34** (2018), No. 2, 1−9.
(12) S. Mataka, K. Takahashi, Y. Ikezaki, T. Hatta, A. Tori-i and M. Tashiro: *Bull. Chem. Soc. Jpn.*, **64** (1991), 68−73.
(13) M. Wang, X. Hu, P. Liu, W. Li, X. Gong, F. Huang and Y. Cao: *J. Am. Chem. Soc*., **133** (2011), 9638−9641.
(14) V. Vohra, K. Kawashima, T. Kakara, T. Koganezawa, I. Osaka, K. Takimiya and H. Murata: *Nature Photonics*, **9** (2015), 403−408.
(15) J. M. Szarko, J. Guo, Y. Liang, B. Lee, B. S. Rolczynski, J. Strzalka, T. Xu, S. Loser, T. J. Marks, L. Yu and L. X. Chen: *Adv. Mater.*, **22** (2010), 5468−5472.
(16) X. Guo, N. Zhou, S. J. Lou, J. W. Hennek, R. P. Ortiz, M. R. Butler, P.-L. T. Boudreault, J. Strzalka, P.-O. Morin, M. Leclerc, J. T. López Navarrete, M. A. Ratner, L. X. Chen, R. P. H. Chang, A. Facchetti and T. J. Marks: *J. Am. Chem. Soc.*, **134** (2012), 18427−18439.